Seasonality of submesoscale dynamics in the Kuroshio Extension

Cesar B. Rocha[1], Sarah T. Gille[1], Teresa K. Chereskin[1], and Dimitris Menemenlis[2]

Key Points.

- Upper-ocean submesoscale (10-100 km) turbulence and inertia-gravity waves undergo strong seasonal cycles that are out of phase.
- Submesoscale turbulence dominates the horizontal velocity and sea-surface height variability in late winter/early spring.
- Submesoscale inertia-gravity waves dominate the horizontal velocity and sea-surface height variability in late summer/early fall.

Two new high-resolution numerical simulations with embedded tides show a strong modulation of near-surface dynamics at submesoscales (roughly 10-100 km) in the Kuroshio Extension. Consistent with recent studies, deep late-winter mixed layers are prone to baroclinic instabilities, and submesoscale turbulence prevails in late winter/early spring. While summertime re-stratification weakens submesoscale turbulence, it also enhances submesoscale inertia-gravity waves near the surface. In the Kuroshio Extension, inertia-gravity waves strongly dominate the submesoscale surface kinetic energy and sea-surface height variance in late summer/early fall.

1. Introduction

Recent interest in upper-ocean dynamics has focused on the strong seasonal cycle of shallow baroclinic instabilities and their role in submesoscale (roughly 1-100 km) turbulence and mesoscale (roughly 100-300 km) modulation [*Sasaki et al.*, 2014; *Qiu et al.*, 2014; *Callies et al.*, 2015; *Thompson et al.*, 2016; *Buckingham et al.*, 2016]. Contemporary studies have also shown that inertia-gravity waves contribute significantly to the near-surface variability at submesoscales [*Richman et al.*, 2012; *Bühler et al.*, 2014; *Rocha et al.*, 2016], but their seasonality has not been investigated.

Using the output of 1/24° and 1/48° global numerical simulations with embedded tides, we show that inertia-gravity waves undergo a strong seasonality near the surface in the Kuroshio Extension region. Interestingly, the seasonal cycle of inertia-gravity waves is out of phase with the seasonal cycle of submesoscale turbulence. On one hand, consistent with previous studies, deep late-winter mixed layers are prone to shallow baroclinic instabilities that are roughly in geostrophic balance and flux energy upscale [*Sasaki et al.*, 2014; *Callies et al.*, 2016], driving a mild seasonal modulation of the mesoscales [*Sasaki et al.*, 2014; *Qiu et al.*, 2014].

Inertia-gravity waves, on the other hand, peak in late summer/early fall, when the upper ocean is strongly stratified. Thus there exists a strong seasonal modulation of upper-ocean submesoscale dynamics: submesoscale turbulence dominates the upper-ocean dynamics in late winter/early, whereas submesoscale inertia-gravity waves prevail in late summer/early fall. Because submesoscale turbulence is weakest in late summer/early fall, the present results indicate that inertia-gravity waves account for most of the summertime submesoscale SSH variability.

2. The LLC numerical simulations

We use the output of two latitude-longitude polar cap (LLC) realistic numerical simulations. The outputs analyzed here, LLC2160 (1/24°) and LLC4320 (1/48°), are forward Massachusetts Institute of Technology general circulation model (MITgcm) numerical solutions on a LLC grid [*Forget et al.*, 2015] with 90-vertical-levels. The coarser-resolution LLC simulation was spun up from an Estimating the Circulation and Climate of the Ocean, Phase II (ECCO2) adjoint-method state estimate, constrained to millions of observations from 2009 through 2011. Both simulations were forced by tides and 6-hourly surface atmospheric fields. The LLC2160 output spans two years from March 2011 to April 2013; the LLC4320 was spun up from the LLC2160 simulation, spanning one year from September 2011 to September 2012. The LLC4320 simulation is an extension of the 3-month long output used by *Rocha et al.* [2016]. Details of the LLC simulations are provided in the supplemental material.

A key aspect of the LLC2160 and LLC4320 simulations is that they were forced by the 16 most-significant tidal components. Because barotropic tides interact with topography and generate internal tides that project onto mesoscales to submesoscales [e.g., *Rocha et al.*, 2016], tidal forcing fundamentally distinguishes our analysis from other modeling studies of seasonality [*Sasaki et al.*, 2014; *Qiu et al.*, 2014].

To study seasonal variations in the upper-ocean dynamics, we focus on the northwest Pacific, in the vicinity of the Kuroshio Extension, where previous studies have shown strong mesoscale and submesoscale seasonality [*Sasaki et al.*, 2014; *Qiu et al.*, 2014]. We analyze a sub-domain of the LLC4320 and LLC2160 simulations of about 2000 km^2 spanning 155-175°E; 25-40°N (Figure 1). The stratification in this mesoscale-rich subtropical region undergoes a vigorous seasonal cycle: wintertime-enhanced small-scale turbulence de-stratifies the upper ocean, yielding mixed layers as deep as 300 m. In late spring/early summer enhanced solar radiation and mixed-layer instabilities re-stratify the upper ocean, yielding mixed layers as shallow as 40 m. Fundamentally, the upper-ocean density structure is well-captured by both LLC simulations: a comparison with Argo climatology shows that both simulations skillfully represent the Kuroshio Extension stratification and its seasonal variability (supplemental material).

[1]Scripps Institution of Oceanography, University of California San Diego, La Jolla, CA, USA.
[2]Earth Sciences Division, Jet Propulsion Laboratory, California Institute of Technology, Pasadena, CA, USA.

0094-8276/16/$5.00

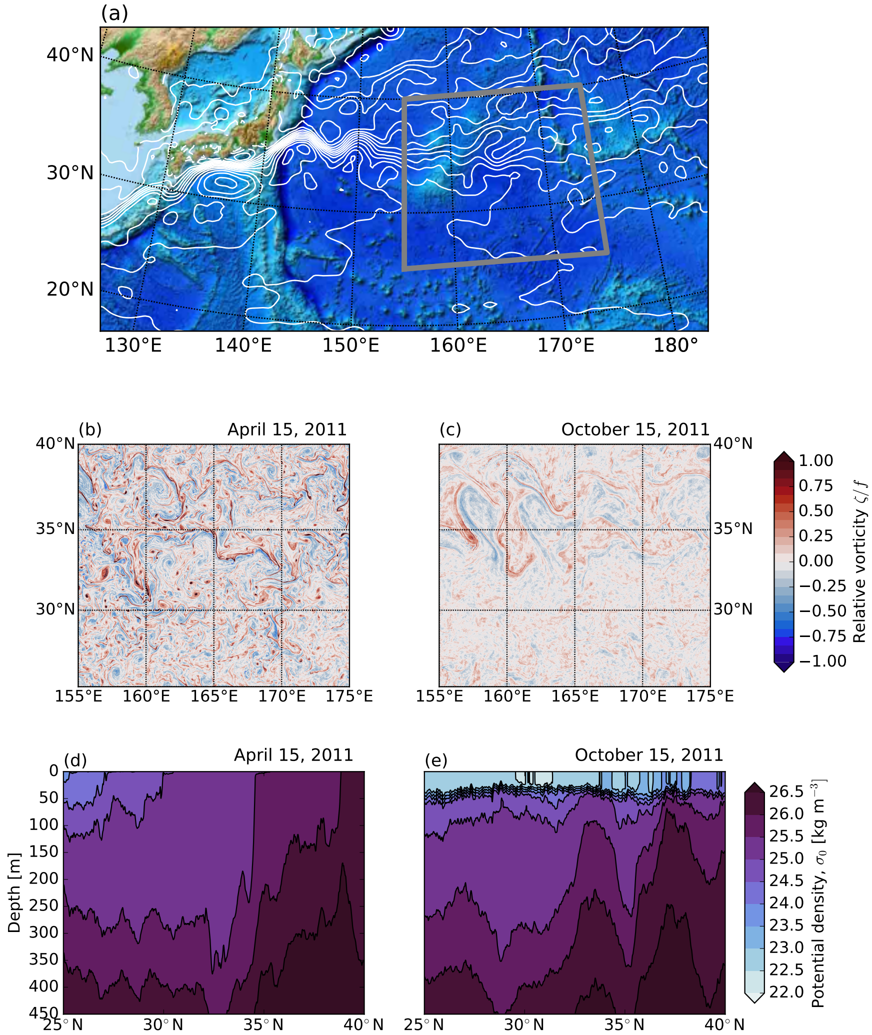

Figure 1. (a) The study region with the subregion where the LLC outputs are analyzed. Colors represent the topography and white lines are contours of absolute dynamic topography every 0.1 m from AVISO. LLC 4320 (1/48°) snapshots of surface vorticity (b and c) and transects of potential density at 165°E (d and e). The snapshots were taken at 00:00 UTC.

3. Statistics of the surface lateral velocity tensor

To study the seasonality in the surface velocity, we calculate the lateral velocity gradient tensor

$$\begin{bmatrix} u_x & u_y \\ v_x & v_y \end{bmatrix} \tag{1}$$

using a centered second-order finite difference scheme. We then diagnose the vertical vorticity

$$\zeta \equiv v_x - u_y \,, \tag{2}$$

lateral rate of strain

$$\alpha \equiv [(u_x - v_y)^2 + (u_y + v_x)^2]^{1/2} \,, \tag{3}$$

and horizontal divergence

$$\delta \equiv u_x + v_y \,. \tag{4}$$

These diagnostics highlight the submesoscale structures in the flow [e.g., *Capet et al.*, 2008; *Shcherbina et al.*, 2013].

Figures 1b-c show snapshots of vertical vorticity ζ in early spring (April 15) and fall (October 15) in the LLC4320 (1/48°) simulation. The model solutions depict seasonality in vorticity: large values of fine-grained vertical vorticity are observed in early spring with maximum values as large as $4f$, where f is the local planetary vorticity, and root-mean-square (RMS) of about $0.4f$. In early fall, the situation is the opposite: the vertical vorticity is relatively coarse-grained; its local maximum and RMS are both smaller than $0.5f$. Indeed, the vorticity and rate of strain are strongest in wintertime (Figure 2): in both simulations, the RMS vorticity and strain rate are about twice as large in late winter/early spring than in late summer/early fall. Because the wintertime vorticity and strain rate are dominated by the smallest scales in the flow (the KE spectra is shallower than a -3 power law in winter), increasing the resolution from $1/24°$ to $1/48°$ increases the wintertime RMS vorticity and strain by about 40%.

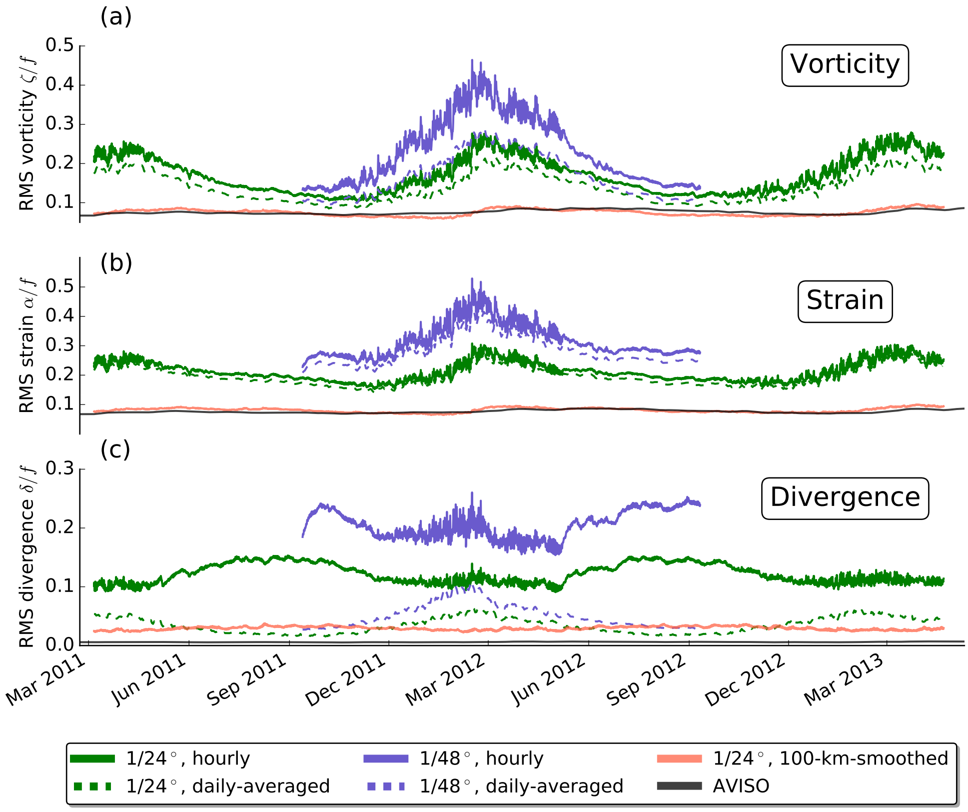

Figure 2. Time series of the root-mean-square (RMS) of (a) vorticity, (b) rate of strain, and (c) horizontal divergence in the LLC outputs and gridded AVISO data.

The bulk of vertical vorticity and strain rate are associated with subinertial flows ($T_f = 2\pi/f_0 \approx 23.5$h, where f_0 is the inertial frequency at the mean latitude): daily-averaging the velocity fields suppresses super-inertial motions and reduces the RMS vorticity by 40% and the RMS strain by 10%; the seasonal cycle remains strong (see dashed lines in figures 2a-b). Indeed, most of this seasonal cycle is associated with submesoscale flows: smoothing the velocity fields with a Hanning filter with cut-off scale of 100 km dramatically reduces the RMS vorticity and strain rate. The reduction in variance is about 80% in winter, yielding RMS vorticity and strain rate roughly consistent with the diagnostics from AVISO gridded geostrophic velocities (compare red lines to black lines in figures 2a-b). The picture that emerges is consistent with recent studies: shallow baroclinic instabilities energize the submesoscales in late winter, drawing from the available potential energy stored in large lateral buoyancy gradients in deep mixed layers [*Sasaki et al.*, 2014; *Callies et al.*, 2015, 2016].

The seasonal cycle of the horizontal divergence, however, showcases the complexity of the upper-ocean annual variability. If submesoscale eddies and fronts dominated the near-surface variability all year, then the seasonal cycle of horizontal divergence, vertical vorticity, and lateral strain rate would be in phase [e.g., *Sasaki et al.*, 2014]. While there is a clear wintertime peak in divergence of daily-averaged velocity (see dashed lines in figure 2c; RMS divergence $\sim 0.1f$ in the $1/48°$ simulation), the hourly fields show a stronger enhancement of lateral divergence in late summer/early fall (RMS divergence $\sim 0.22f$ the $1/48°$ simulation). Because the $1/48°$ simulation better resolves smaller-scale submesoscale flows, a secondary RMS divergence peak in winter is nearly as strong as in summer. Submesoscale fronts and eddies evolve relatively fast, and there is no clear temporal and spatial scale separation between those motions and inertia-gravity waves [*McWilliams*, 2016]: daily-averaging the velocity fields efficiently suppresses the summertime horizontally divergent flows, but also reduces the wintertime lateral divergence by about 50%. Figure 2c also shows that most of the lateral divergence is associated with submesoscale flows: smoothing the velocity fields with a 100-km-cutoff suppresses more than 80% of the RMS divergence.

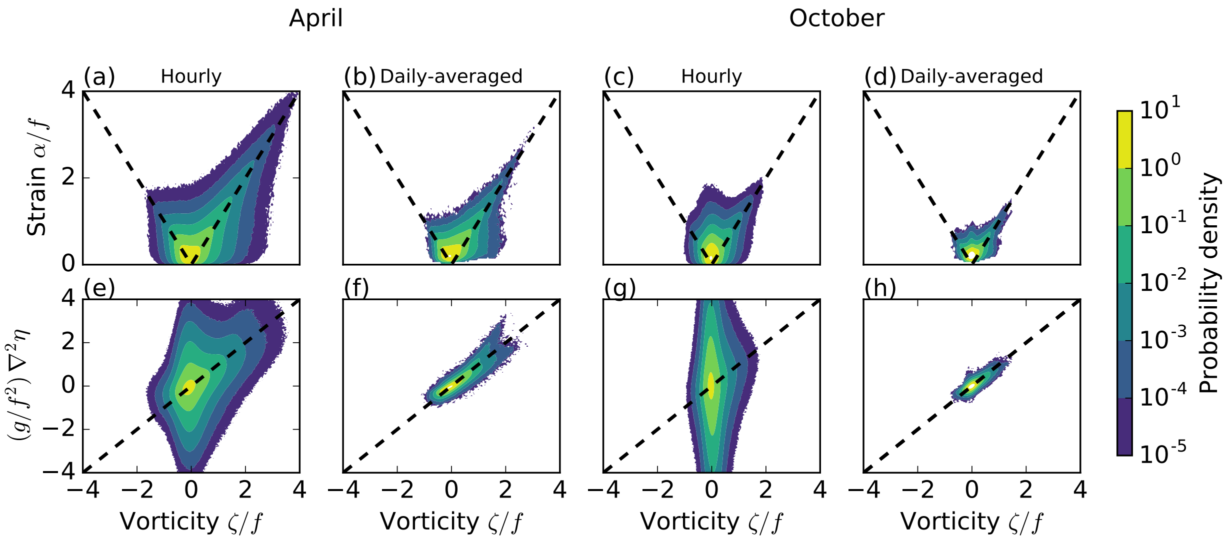

Figure 3. Seasonal variation of joint probability distributions: vorticity vs. strain rate (a through d), and vorticity vs. Laplacian of sea-surface height (e through h) in April (a, b, e, f) and October (c, d, g, h). Dashed lines in (a) through (d) represent one dimensional shear flow $\alpha = \pm\zeta$, characteristic of fronts. Dashed lines in (e) through (h) represent geostrophic flow $\zeta = \frac{g}{f}\nabla_h^2\eta$.

4. Seasonality of submesoscale dynamics

The results of figure 2a-c show that submesoscale surface variability stems from different dynamics in summer than in winter. To characterize these differences, we calculate joint probability distributions (jPDF) of vorticity-strain and vorticity-Laplacian of sea-surface height (Figure 3).

The April vorticity-strain jPDF has a shape characteristic of submesoscale turbulence (Figures 3a-b). The alignment of vorticity and strain $\alpha \sim \pm\zeta$ with strong positive skewness are fingerprints of submesoscale fronts [*Shcherbina et al.*, 2013; *McWilliams*, 2016]. The shape of the vorticity-strain jPDF is similar for hourly and daily-averaged fields, although the vorticity skewness reduces from 1.4 to 1.13 from hourly to daily-averaged. The April results are characteristic of winter, indicating that wintertime submesoscale surface velocity is strongly dominated by submesoscale turbulence. The hourly velocity fields are significantly ageostrophic as depicted by the jPDF of vorticity-Laplacian of SSH winter (Figure 3e). Even in April, only the daily-averaged fields are largely in geostrophic balance (the jPDF of daily-averaged vorticity vs.

Laplacian of SSH is an ellipse with large eccentricity and main axis tilted by 45°; Figure 3f).

The October vorticity-strain jPDF shows much weaker skewness (the vorticity skewness is 0.68 and 0.67 for hourly and daily-averaged velocities). The shape of the vorticity-strain jPDF appears to be a combination of two half-ellipses centered about $\zeta = 0$, one with a 45° slope (characteristic of submesocale fronts that persist in summer) and one with a very steep slope. That the submesoscale dynamics in October are mainly unbalanced is clearly depicted in the shape of jPDF of vorticity-Laplacian of SSH for hourly fields (Figure 3g), which is an ellipse aligned in the vertical axis. Daily-averaging the model suppresses the ageostrophic, super-inertial flows, and, therefore, the daily-averaged flow is essentially geostrophic as depicted by the 45°-tilted ellipse in the vorticity-Laplacian of SSH jPDF.

Time series of PDFs of vorticity and divergence (supplemental material) show a strong oscillation between these two regimes. In late winter/early spring the vorticity is strongly positively skewed, whereas the divergence is moderately negatively skewed as predicted by frontogenesis [e.g., *Capet et al.*, 2008; *McWilliams*, 2016] . In late summer/early fall, the divergence is stronger, but PDFs are much less skewed, consistent with linear inertia-gravity waves.

5. Projection onto horizontal scales

To better quantify the projection of these flows onto different horizontal scales, we calculate wavenumber spectra of kinetic energy and sea-surface height (SSH) variance. Before calculating the spectra, time-mean and spatial linear trends were removed, and the resulting fields were multiplied by a two-dimensional Hanning "spectral window". The two-dimensional spectra were averaged azimuthaly [e.g., *Rocha et al.*, 2016] . We discuss only spectra for the 1/48° simulation, which extends the 1/24° simulation towards smaller scales (supplemental material).

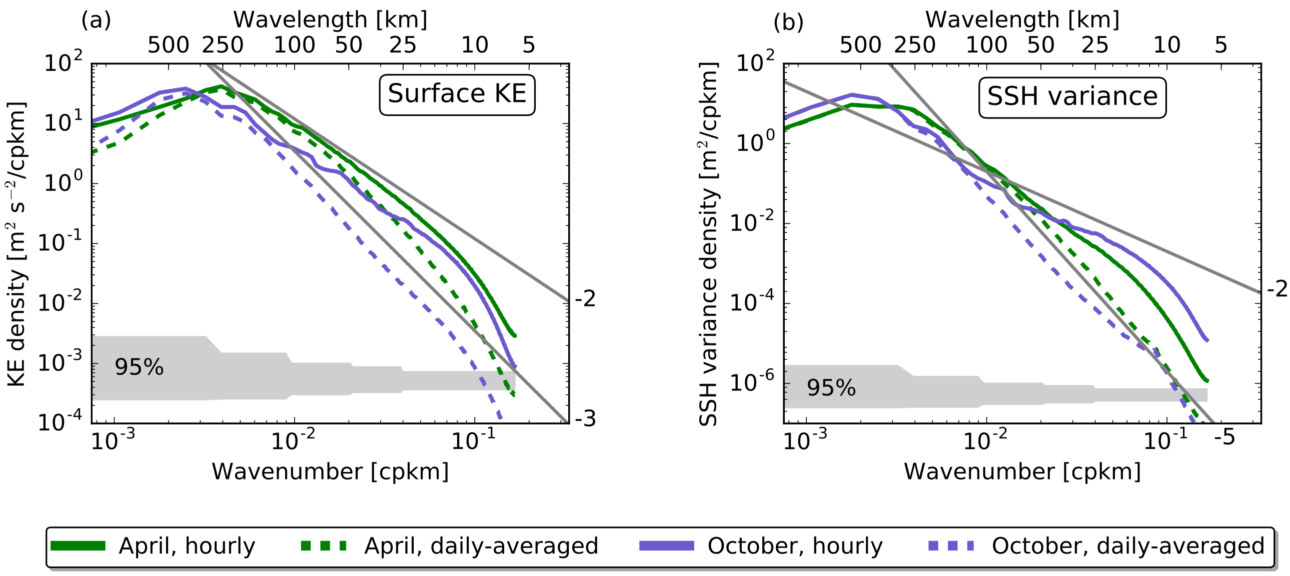

Figure 4. Surface (horizontal) KE (a) and SSH variance wavenumber spectra (b) in the 1/48° simulation. Solid lines are spectra based on hourly snapshots, and dashed lines are spectra based on daily-averaged fields.

Figure 4a depicts the horizontal wavenumber spectra of surface KE in April and October. At scales larger than 20km, the April and October spectra based on hourly velocity snapshots (solid lines) are nearly indistinguishable from each other within 95% confidence level. Consistent with the results of *Rocha et al.* [2016], who analyzed a 3-month output of the LLC4320 simulation in Drake Passage, there is significant high-frequency variabilty at submesoscales. Daily-averaging the velocity field suppresses spatial variability at scales smaller than about 250 km, both in April and October (compare solid lines against dashed lines in Figure 4a). But this suppression is dramatic in October, when the inertia-gravity waves peak. At scales smaller than 100 km, 39% of the surface KE in April is accounted for by super-inertial flows as opposed to 79% in October. The seasonality of subinertial submesoscale flows is more dramatic than the seasonal cycle of the total flow. This is consistent with the results of *Sasaki et al.* [2014], which are based on daily-averaged velocity fields of a different model without tidal forcing (P. Klein, personal communication).

The inertia-gravity waves project on the sea-surface. There is a dramatic difference between the spectra based on hourly and daily-averaged SSH in October (Figure 4b): at scales smaller than 100 km, the spectra of hourly SSH roughly follows a -2 power-law, whereas the spectra of daily-averaged SSH roughly follows a -5 power-law. At these scales, 33% of the SSH variance in April is accounted for by super-inertial flows as opposed to 83% in October! Curiously, the out-of-phase seasonal cycle of submesoscale turbulence and near-surface submesoscale inertia-gravity waves conspire to yield weak seasonality in the spectra of KE and SSH variance based on hourly fields.

6. Summary and Conclusion

Our work adds to recent studies that present modeling [*Sasaki et al.*, 2014] and observational [*Callies et al.*, 2015; *Buckingham et al.*, 2016] evidence of vigorous seasonality in submesoscale turbulence. In particular, our main finding is that in global simulations with embedded tides the near-surface submesoscale inertia-gravity waves in the Kuroshio Extension undergo a strong seasonal cycle that is out-of-phase with the seasonal cycle of submesoscale turbulence. We conjecture that the summertime dominance of inertia-gravity waves [*Callies et al.*, 2015] is a consequence both of suppression of submesoscale turbulence and enhancement of inertia-gravity waves due to re-stratification of the upper ocean.

D'Asaro [1978] showed that the velocity of linear internal waves in the mixed layer strongly depends on the density jump at the mixed-layer base, with largest mixed layer velocities when the jump is strongest. In summer, the shallow mixed layer overlays a strong seasonal pycnocline, and thus the internal waves projection onto the mixed-layer may be stronger according to *D'Asaro* [1978]'s arguments. An alternative explanation is that the shape of the baroclinic modes changes seasonally. In particular the baroclinic modes are significantly more surface intensified in late summer/early fall (supplemental material). If the internal wave source has weak seasonal dependence, then a strong seasonal cycle in the near-surface expression of internal waves is expected. Internal tide generation does not show a seasonal modulation [e.g., *Alford*, 2003], and therefore one expects a strong seasonality in the near-surface expression of internal tides and other submesoscale inertia-gravity waves generated through internal tide interactions. Near-inertial wave generation peaks in winter [e.g., *Alford*, 2003], but those waves project on large horizontal scales [e.g, *Qi et al.*, 1995].

An important caveat is that this study focuses on a single patch of ocean in the vicinity of the Kuroshio Extension. This may be typical of a mesoscale-rich subtropical region, but it is unlikely to be representative of other regions such as low-eddy-kinetic-energy eastern boundary currents and the middle of the subtropical gyre. We plan to report on the geographic variability of submesoscale seasonality in a future study.

Acknowledgments. William R. Young provided helpful feedback on the first draft. We thank the MITgcm community and our colleagues at the NASA Advanced Supercomputing (NAS) Division for their awesome support. This research was funded by NSF (OCE1357047) and NASA (NNX13AE44G,NNX13AE85G,NNX16AH67G). The LLC output can be obtained from the ECCO project (`http://ecco2.org/llc_hires`). The altimeter products were produced by Ssalto/Duacs and distributed by Aviso, with support from CNES (`http://www.aviso.altimetry.fr/duacs/`).

References

Alford, M. H. (2003), Redistribution of energy available for ocean mixing by long-range propagation of internal wave, *Nature*, *423*(6936), 159–162.

Buckingham, C. E., A. C. Naveira Garabato, A. F. Thompson, L. Brannigan, A. Lazar, D. P. Marshall, A. George Nurser, G. Damerell, K. J. Heywood, and S. E. Belcher (2016), Seasonality of submesoscale flows in the ocean surface boundary layer, *Geophysical Research Letters*, *43*(5), 2118–2126.

Bühler, O., J. Callies, and R. Ferrari (2014), Wave–vortex decomposition of one-dimensional ship-track data, *Journal of Fluid Mechanics*, *756*, 1007–1026.

Callies, J., R. Ferrari, J. M. Klymak, and J. Gula (2015), Seasonality in submesoscale turbulence, *Nature communications*, *6*.

Callies, J., G. Flierl, R. Ferrari, and B. Fox-Kemper (2016), The role of mixed-layer instabilities in submesoscale turbulence, *Journal of Fluid Mechanics*, *788*, 5–41.

Capet, X., J. C. McWilliams, M. J. Molemaker, and A. Shchepetkin (2008), Mesoscale to submesoscale transition in the California Current System. Part I: Flow structure, eddy flux, and observational tests, *Journal of Physical Oceanography*, *38*(1), 29–43.

D'Asaro, E. A. (1978), Mixed layer velocities induced by internal wave, *Journal of Geophysical Research: Oceans*, *83*(C5), 2437–2438.

Forget, G., J.-M. Campin, P. Heimbach, C. Hill, R. Ponte, and C. Wunsch (2015), ECCO version 4: an integrated framework for non-linear inverse modeling and global ocean state estimation, *Geosci. Model Dev.*, *8*, 3071–3104.

McWilliams, J. C. (2016), Submesoscale currents in the ocean, in *Proc. R. Soc. A*, vol. 472, p. 20160117, The Royal Society.

Qi, H., R. A. De Szoeke, C. A. Paulson, and C. C. Eriksen (1995), The structure of near-inertial waves during ocean storms, *Journal of Physical Oceanography*, *25*, 2853–2871.

Qiu, B., S. Chen, P. Klein, H. Sasaki, and Y. Sasai (2014), Seasonal mesoscale and submesoscale eddy variability along the North Pacific Subtropical Countercurrent, *Journal of Physical Oceanography*, *44*(12), 3079–3098.

Richman, J. G., B. K. Arbic, J. F. Shriver, E. J. Metzger, and A. J. Wallcraft (2012), Inferring dynamics from the wavenumber spectra of an eddying global ocean model with embedded tides, *Journal of Geophysical Research: Oceans*, *117*(C12).

Rocha, C. B., T. K. Chereskin, S. T. Gille, and D. Menemenlis (2016), Mesoscale to submesoscale wavenumber spectra in Drake Passage, *Journal of Physical Oceanography*, *46*, 601–620.

Sasaki, H., P. Klein, B. Qiu, and Y. Sasai (2014), Impact of oceanic-scale interactions on the seasonal modulation of ocean dynamics by the atmosphere, *Nature communications*, *5*.

Shcherbina, A. Y., E. A. D'Asaro, C. M. Lee, J. M. Klymak, M. J. Molemaker, and J. C. McWilliams (2013), Statistics of vertical vorticity, divergence, and strain in a developed submesoscale turbulence field, *Geophysical Research Letters*, *40*(17), 4706–4711.

Thompson, A. F., A. Lazar, C. Buckingham, A. C. Naveira Garabato, G. M. Damerell, and K. J. Heywood (2016), Open-ocean submesoscale motions: A full seasonal cycle of mixed layer instabilities from gliders, *Journal of Physical Oceanography*, *46*(4), 1285–1307.

Corresponding author: Cesar B. Rocha, Scripps Institution of Oceanography, University of California San Diego, La Jolla, CA, USA. (crocha@ucsd.edu)